Calibration of oxygen buffers at elevated *P* and *T* using the hydrogen fugacity sensor

I-Ming Chou

SN7, Geochemistry Branch
NASA Johnson Space Center
Houston, Texas 77058

Abstract

An internally-consistent set of data for the oxygen-fugacity buffers magnetite–hematite (MH), manganosite–hausmannite ($MnO-Mn_3O_4$), nickel–nickel oxide (NNO), fayalite–magnetite–quartz (FMQ), and cobalt–cobalt oxide (Co–CoO) at 1 atm has been obtained by using the hydrogen-fugacity sensor technique of Chou and Eugster (1976a) at 2 and 4 kbar total pressures between 600° and 800°C.

Using the fO_2 values given by Huebner and Sato (1970) for NNO buffer as a reference, the data can be represented by the following equations (at 1 atm) with *T* in K:
For MH buffer:

$$\log fO_2\ (\pm 0.12) = 0.0260 + 0.4381\ (10^4/T) - 0.1572\ (10^4/T)^2 \text{ for } 1073 \geq T \geq 873,$$

$$\text{and } \log fO_2\ (\pm 0.12) = (-26629/T) + 15.288 \text{ for extrapolation to } T \geq 1073;$$

for $MnO-Mn_3O_4$ buffer:

$$\log fO_2\ (\pm 0.12) = (-25793/T) + 13.714;$$

for FMQ buffer:

$$\log fO_2\ (\pm 0.08) = (-23973/T) + 7.985 \text{ for } T \geq 873;$$

and for Co–CoO buffer:

$$\log fO_2\ (\pm 0.08) = (-24391/T) + 7.382.$$

The present fO_2 values for $MnO-Mn_3O_4$ and Co–CoO buffers are in good agreement with those of Huebner and Sato (1970) and Robie and Waldbaum (1968) respectively. However, for MH and FMQ buffers, the present fO_2 values are consistently lower and higher respectively than those reported previously. The difference can be minimized if the values of Gibbs free energy of formation for magnetite are 0.68, 0.35, and 0.17 kcal/mole less negative than those reported by Haas and Robie (1973) at 900, 1100, and 1300 K respectively.

Introduction

The oxygen-buffer technique developed by Eugster (1957) has been applied extensively to study mineral–gas equilibria of igneous and metamorphic reactions (Eugster and Wones, 1962; Huebner, 1971). Recently the acid-base buffer technique (Frantz and Eugster, 1973; Chou and Eugster, 1976b) makes it possible to measure quantitatively the equilibrium constants for reactions between minerals and the coexisting super-critical aqueous solutions (Frantz, 1973; Gunter, 1974; Chou and Eugster, 1976b; Chou and Eugster, 1977; Gunter and Eugster, in press).

To obtain a set of reliable thermodynamic data for minerals as well as aqueous species using the buffer techniques, we first have to have a set of internally consistent data for the oxygen buffers. The importance of the latter is demonstrated by Eugster and Wones (1962), Wones and Eugster (1965) and Wones (1972), and emphasized by Zen (1977). The internal consistency of the data for the oxygen buffers is tested

in this study by using the hydrogen-fugacity sensor technique of Chou and Eugster (1976a). The hydrogen fugacity, $f\mathrm{H}_2$, has been measured at 2 and 4 kbar total pressures and from 600° to 800°C for the assemblage $\mathrm{H}_2\mathrm{O}$ + oxygen buffer. The buffers examined include MH (magnetite–hematite), MnO–$\mathrm{Mn}_3\mathrm{O}_4$ (manganosite[1]–hausmannite), NNO (nickel–nickel oxide), FMQ (fayalite–magnetite–quartz), and Co–CoO (cobalt–cobalt oxide).

The hydrogen fugacity sensor

The Ag–AgCl–$\mathrm{H}_2\mathrm{O}$–HCl acid buffer of Frantz and Eugster (1973) can be used as a $f\mathrm{H}_2$ sensor at elevated P and T by enclosing the acid-buffer assemblage in a small Pt capsule and placing the capsule within a larger volume of another system, the $f\mathrm{H}_2$ of which is to be measured. In this arrangement the external system controls the $f\mathrm{H}_2$ of the sensor assemblage, as hydrogen permeates through the Pt capsule wall easily at elevated temperatures. For the reaction, assuming pure solids and pure liquid AgCl,

$$\mathrm{Ag(s)} + \mathrm{HCl\,(g)} = \mathrm{AgCl\,(s\ or\ l)} + 1/2\ \mathrm{H}_2\mathrm{(g)}, \quad (1)$$
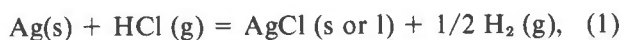
$$(K_1)^2_{P,T} = f\mathrm{H}_2^{1/2} / f\mathrm{HCl}. \quad (2)$$

If the $f\mathrm{H}_2$ is externally imposed, the fugacity of HCl and hence the concentration of HCl in the fluid is fixed at given P and T at equilibrium. Since in the P-T region of this study HCl is mostly associated (Frank, 1956; Frantz and Eugster, 1973; Helgeson and Kirkham, 1976), and it dissociates completely upon quenching, the HCl concentration of the fluid in the sensor capsule at P and T can be determined by measuring pH or the concentration of chloride ion after quench;

$$(m\mathrm{HCl}/_{P,T}) = (m\mathrm{H}^+)_{1+25°\mathrm{C}} = (m\mathrm{Cl}^-)_{1,25°\mathrm{C}} \quad (3)$$

where m_i is the molality (number of moles/1000 g of $\mathrm{H}_2\mathrm{O}$) of i.

If Lewis and Randall's rule (Lewis and Randall, 1923) is obeyed for the $\mathrm{H}_2\mathrm{O}$–HCl fluid at P and T, the $(f\mathrm{H}_2)_{P,T}$ in the sensor and the outer system can be obtained from equations (2) and (3):

$$(f\mathrm{H}_2)_{P,T} = [(K_4)_{P,T} \cdot (m\mathrm{H}^+)_{1,25°\mathrm{C}}]^2$$

$$= [(K_4)_{P,T} \cdot (m\mathrm{Cl}^-)_{1,25°\mathrm{C}}]^2 \quad (4)$$

in which $(K_4)_{P,T} = (K_1)_{P,T} \cdot P^*_{\mathrm{HCl}} \cdot \gamma^*_{\mathrm{HCl}} / 55.5$

where P^*_i and γ^*_i are the partial pressure and fugacity coefficient of pure i at P and T. The detailed thermodynamic derivations for equation (4) are given in Appendix A.[3]

From the measured $m\mathrm{H}^+$ or $m\mathrm{Cl}^-$, $(f\mathrm{H}_2)_{P,T}$ of the outer system can be calculated from equation (4) provided $(K_4)_{P,T}$ is known. Since the values of $(K_4)_{P,T}$ calculated from the available thermodynamic data contain large uncertainties, it is essential to calibrate these values experimentally before equation (4) can be applied. The method and results of the calibration will be given later.

In order to assure the attainment of equilibrium at elevated P and T, two sensor capsules with different initial concentrations (Fig. 1), one (sensor A) smaller and the other (sensor B) larger than the final equilibrated HCl concentration, are used. The closeness of the final HCl concentrations in the two capsules is considered to reflect the degree of attainment of equilibrium (see Appendix A). As the diffusion of H_2 through the Pt capsule is probably the rate-determining step for the equilibration, these concentrations reflect the high temperature and pressure equilibrium. A schematic diagram showing the experimental arrangement and conceptualized $f\mathrm{H}_2$ change as the system approaches equilibrium is given in Figure 1.

Experimental apparatus and procedures

The experimental procedures are similar to those of Frantz and Eugster (1973), Chou and Eugster (1976b), and Chou and Frantz (1977). To prepare sensors A and B of Figure 1, 15 to 20 μl of solution, either distilled $\mathrm{H}_2\mathrm{O}$ or 3M HCl, together with ~20 mg Ag and ~20 mg AgCl were loaded into a Pt capsule, 1.85 mm OD, 1.54 mm ID, 19 mm long, which was then welded shut. Both capsules were flattened, using a pair of pliers, and placed with the oxygen buffer and 30 to 50 μl $\mathrm{H}_2\mathrm{O}$ into a Au capsule, 4.4 mm OD, 4.0 mm ID, 25 mm long, which was in turn welded shut.

Conventional 30.5 cm cold-seal pressure vessels with rapid-quench attachments were used for 2 kbar total pressure runs. In order to minimize the temperature gradient, argon was used as a pressure medium (Rudert et al., 1976), and the pressure vessels were placed horizontally in split furnaces with a 5.8 cm filler rod resting against the charge to minimize

---

[1] This phase is nonstoichiometric, but will be represented by MnO in this paper for sake of convenience.

[2] $(K_i)_{P,T}$ represents the equilibrium constant of reaction i at P and T.

[3] To obtain a copy of the appendices to this paper, order Document AM–78–074 from the MSA Business Office, 1909 K Street, NW, Washington, DC 20006. Please remit $1.00 in advance for the microfiche.
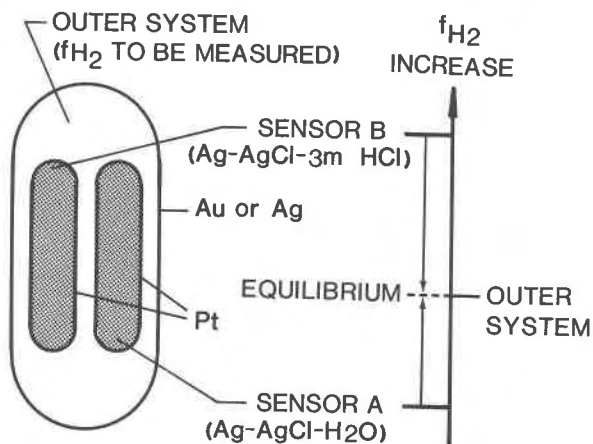
Fig. 1. A schematic diagram showing the experimental arrangement and conceptualized fH_2 change as the system approaches equilibrium. For details see text.

convection. Furnace power was controlled by a solid-state temperature controller, using a Pt sensing element mounted inside the furnace windings. Temperature was measured by a conventional potentiometer using sheathed chromel–alumel thermocouples, which were calibrated against the melting points of NaCl, KCl, and Zn at 1 atm. The temperature gradient across the charge, calibrated by the method of Rudert *et al.* (1976), is less than 3°C. Two Heise gauges were used to monitor the pressure within the uncertainties of ±7 bar. The duration of the runs at 800°, 700°, and 600°C are 1, 2, and 4 days respectively.

At the conclusion of the equilibration period the charge was quenched by tipping the bomb and letting the charge capsule slide at pressure to the cold end of the bomb.

Runs at 4 kbar were performed using internally-heated pressure vessels with Mo-wound furnace and a six-hole Mo sample holder. Argon was used as the pressure medium. The pressure was recorded by a Foxboro dynalog, which was calibrated against a Heise gauge to the accuracy of ±50 bar. Furnace power was controlled with a solid-state controller. Temperature was recorded on a strip-chart recorder using a sheathed Pt + 10 percent Rh–Pt thermocouple; the system was calibrated against the melting points of Au, NaCl, KCl, and Zn at 1 atm. Temperatures reported are believed to be accurate to better than ±5°C. The duration of the runs at 800°, 700°, and 600°C are 1/3, 2, and 4 days respectively.

At the conclusion of each equilibration period, the charges were quenched by turning off the power sup-

ply. The temperature dropped from 600° to lower than 200°C within three minutes.

Capsules were removed, cleaned, and weighed. The presence of fluid phase in the external system was carefully determined using a hot-plate test; any dry capsule was discarded. To ascertain that all solid buffer phases were present, the buffers were examined optically and/or by X-ray diffraction. The inner sensor capsules were cleaned and pierced on a teflon plate with a tungsten carbide needle. 3 to 10 μl solution were removed using a microcapacity disposable pipet, and chloride content was then determined coulometrically with a Buchler Digital chloridometer. Although the experimental procedures are similar to those of Chou and Frantz (1977), the following improvements have been made:

(1) Two sensor capsules were exposed to the same external system, therefore the equilibration of the system can be demonstrated in a single run.

(2) Shorter capsules were used to minimize the temperature gradient across the sample charge.

(3) Smaller amounts of solutions were loaded in the inner capsules to minimize the total hydrogen transfer across the Pt membrane required for the system to reach equilibrium (Chou *et al.*, 1978) and shorten the equilibration period.

Starting materials used in this study, together with their sources and methods of preparation, are listed in Table 1.

Experimental results

As stated earlier, using the measured $(mCl^-)_{1,25\,°C}$ and equation (4) to calculate $(fH_2)_{P,T}$, it is necessary to calibrate $(K_4)_{P,T}$. This is achieved by using a well-calibrated fH_2 buffer in the external system and measuring $(mCl^-)_{1,25\,°C}$ of the quenched solutions in sensors A and B after the system reaches equilibrium at P and T. The Ni + NiO + H_2O assemblage was used as the fH_2 buffer for this purpose for the following reasons: (1) the assemblage has a rapid reversibility; (2) oxygen fugacity–temperature relations for the Ni + NiO assemblage have been determined electrochemically by Huebner and Sato (1970) at 1 atm total pressure and over the temperature range 519°–1319°C. Their data are in good agreement with those of other investigators using different methods; (3) the assemblage provides a good reference for the calibration of the other buffer assemblages in this study, as its fH_2 values are intermediate to the range of fH_2 values of the other buffers.

The $\log fO_2$ values listed in Table 2 are calculated from the equation given by Huebner (1971). Values

Table 1. Preparation of starting materials

Starting Material	Source and/or method of preparation
Magnetite	Fisher purified Fe_3O_4 (Lot # 742965).
Hematite	Matheson Coleman and Bell (99% Fe_2O_3 assay min.).
Manganosite	Fisher certified MnO_2 (100.7%) was reduced in a stream of hydrogen at 800°C for 15 hours.
Hausmannite	Fisher certified MnO_2 was heated in air at 1100°C for 20 hours.
Nickel	City Chemical Corp., New York (99.25% Ni, 200 mesh).
Bunsenite	Baker analyzed reagent (Lot # 32479).
Fayalite	(1) Gas mixing furnace method: A mix of ultra pure iron sponge (99.999% Fe, Research Organic/Inorganic Chem. Corp.) and α-cristobalite (prepared from Fisher certified silicic acid, lot # 732108) was pelletized and placed in an alumina container and reacted in a gas mixing furnace for 3 days at 1100°C and log f_{O_2} = -11.5, which was controlled by mixing CO and CO_2, monitored by a $(ZrO_2)_{0.85}$ $(CaO)_{0.15}$ ceramic oxygen electrolyte cell (Sato, 1971; Williams and Mullins, 1976). The sample was quenched and ground, and the procedures repeated several times. (2) Hydrothermal method: A mix of $FeC_2O_4 \cdot 2H_2O$ (Matheson Coleman and Bell purified) and α-cristobalite together with H_2O were welded into a Pt or AgPd tube, which together with H_2O and Co-CoO buffer were in turn welded into an Au tube. The assemblage was loaded in a conventional cold-seal bomb and reacted at 2 kb, 700°C for a week. Some pure fayalite was synthesized in a Au capsule without using an external buffer.
Quartz	Natural quartz from Lake Tuxaway.
Cobalt	SPEX Industries, Ind. (Lot #04761).
Cobalt oxide	Baker analyzed $Co(NO_3)_2 \cdot 6H_2O$ (lot # 3650) was heated at 1100°C for 7 hours.
Ag	Fisher certified Reagent (Lot # 723248).
AgCl	Baker analyzed reagent (Lot # 29310).
HCl	Diluted from the concentrated HCl of Shape Products Co. (Lot #1539).

for log fH_2 are calculated from fH_2O data of Burnham *et al.* (1969) and the dissociation constant of H_2O, K_w in equation A-2 of Appendix A, of Robie and Waldbaum (1968). Listed values for $(mCl^-)_{1,25°C}$ are the averages of those in Tables B-1 and B-2 of Appendix B. The calibrated $(K_4)_{P,T}$ values are given in Table 2.

Since the values of $(mHCl)_{P,T}$ are important for the mineral solubility measurements using Ag–AgCl–H_2O–HCl acid buffer technique (Frantz and Eugster, 1973; Chou and Eugster, 1977; Gunter and Eugster, in press), they are given in Tables B-1 and B-2 (Appendix B) as $(mCl^-)_{1,25°C}$ [see equation (3)] for runs at 2 and ~4 kbar respectively. Each listed number represents one measurement. Two sets of data are given for each run; the first set is for sensor A and the second for sensor B. The uncertainties of measurements for log $(mCl^-)_{1,25°C}$ are ±0.02 for MH and MnO–Mn_3O_4 buffers and ±0.01 for NNO, FMQ, and Co–CoO buffers. Results are plotted in Figures 2 (2 kbar) and 3 (4 kbar). Triangles with the apices pointing up and pointing down represent the average values for sensors A and B respectively. Results of least-squares refinements of log $(mHCl)_{P,T}$ *vs.* $1/T$[4] are given in Table 3 and plotted in Figures 2 and 3 as solid lines, with dashed curves indicating the 95 percent confidence limits of the regression. The scatter-

[4] In this paper, T is in K unless otherwise indicated

Table 2. Calibration of $(K_4)_{P,T}$

P (kb)	T (°C)	log f_{O_2} [1]	log f_{H_2O} [2]	log f_{H_2} [3]	log $(m_{Cl^-})_{1,25°C}$ [4]	log $(K_4)_{P,T}$ [5]
2	600	-19.091	3.020	0.584	-0.407	0.698
2	650	-17.550	3.079	0.687	-0.302	0.646
2	700	-16.167	3.128	0.762	-0.225	0.605
2	750	-14.920	3.167	0.836	-0.136	0.554
2	800	-13.788	3.198	0.890	-0.043	0.488
4.020	600	-18.985	3.338	0.848	-0.435	0.859
4.000	650	-17.451	3.396	0.953	-0.416	0.893
4.033	650	-17.449	3.401	0.957	-0.387	0.865
4.055	700	-16.070	3.455	1.040	-0.336	0.856
4.080	750	-14.826	3.501	1.123	-0.266	0.828
4.110	750	-14.825	3.505	1.126	-0.239	0.802
4.070	800	-13.699	3.535	1.184	-0.181	0.773

1) Calculated from Huebner (1971).

2) Calculated from the data given by Burnham, Holloway, and Davis (1969).

3) Calculated from eq. (A-2), using $(K_w)_T$ values of Robie and Waldbaum (1968).

4) Average of the values given in tables B-1 and B-2.

5) For definition and calculation, see eq. (4).

Table 3. Calculations for the acid buffer O_B, OH (AgAgCl, HOCl)*, log $(mHCl)_{P,T} = A/T + B$

Oxygen Buffer	A	B	No. of Data Points	Standard Error of A	Standard Error of B
(a) P = 2 kb					
MnO-Mn₃O₄	-1522	0.448	16	105	0.109
NNO	-1640	1.471	14	28	0.029
FMQ	-2023	1.943	10	53	0.055
Co-CoO	-1791	1.974	8	72	0.074
(b) P = ~4 kb					
MnO-Mn₃O₄	-1027	-0.151	16	108	0.112
NNO	-1258	0.980	18	68	0.068
FMQ	-1362	1.139	12	47	0.050
Co-CoO	-1319	1.399	8	36	0.037

*For details of buffer notation see Eugster and Skippen (1967).

ing of data points for ~4 kbar runs is due to the slight pressure variations among the runs (see Table B-2). Data for the MH buffer were not fitted with linear equations because the enthalpy of the reaction is not a constant over the temperature interval investigated (Fig. 4). This is due to the phase transitions of magnetite (~900 K) and hematite (~950 K) (Robie and Waldbaum, 1968). The effect of the magnetite transition on FMQ is small and can be neglected. The data for MH buffer can be represented by the following polynominal equations for $1073 \geq T \geq 873$:

2 kbar: log $mHCl = 14.538 - 3.7130(10^4/T)$

$$+ 0.28285(10^4/T)^2 - 0.006927(10^4/T)^3 \quad (5)$$

4 kbar: log $mHCl = 99.271 - 28.7228(10^4/T)$

$$+ 2.72903(10^4/T)^2 - 0.086283(10^4/T)^3 \quad (6)$$

The agreement between the data presented here and those reported earlier (Chou and Frantz, 1977) is good, even though the present values are consistently lower in $(mCl^-)_{1,25°C}$. The small discrepancy is due to the improvements of both the physical set-up for the experiments and the analytical procedures discussed above. Values given in Tables B-1 and B-2 for log $(fO_2)_{P,T}$ are calculated from equations (A-2) and (4) using $(K_4)_{P,T}$ of Table 2, and for log $(fO_2)_{1,T}$ are obtained by using the pressure correction procedure of Eugster and Wones (1962)[5]. Average values for log $(fO_2)_{1,T}$ derived from 2 kbar and 4 kbar data are

---

[5] For the buffer reactions (8), (18), (22), (26), and $2NiO(s) = 2Ni(s) + O_2(g)$, ignoring the compressibilities and thermal expansions of the solids involved,

log $(fO_2)_{1,T} = $ log $(fO_2)_{P,T} + (\Delta Vs/2.303R) \cdot (P-1)/T$

where ΔVs is the volume change of the reaction for solids. The molar volume data for solids are from Robie and Waldbaum (1968), and the coefficients for the pressure correction term for various buffers are given in Table 6.

---

summarized in Table 4, and the agreement between these two sets of data is excellent.

Extrapolations and thermodynamic values

To extrapolate and derive thermodynamic values for buffer reactions (8), (18), (22), and (26), assuming pure solids, the relation

$$[\partial(\log fO_2)/\partial(1/T)]_{1 \text{ atm}} = -\Delta H_r^0/2.303 \, R \quad (7)$$

can be used, provided the standard enthalpy of reaction at 1 atm and T, ΔH_r^0, is a constant or has a small variation over the range of temperatures investigated. Values of ΔH_r^0 for the buffer reactions are calculated from the data of the enthalpy of formation, ΔH_f^0, given by Robie and Waldbaum (1968), and are plotted in Figure 4. The data for the MH and FMQ buffers in this report are evidently not suitable for extrapolation to both lower and higher temperatures and lower temperatures respectively.

MH buffer

Using pure solid at P and T and pure gas at 1 bar and T as standard states for solids and gases respectively, for the reaction

$$6 \, Fe_2O_3(s) = 4 \, Fe_3O_4(s) + O_2(g), \quad (8)$$

$$K_8 = (a_{Fe_3O_4}^4 \cdot aO_2)/a_{Fe_2O_3}^6 = fO_2 \quad (9)$$

for pure solids. The fO_2 data for MH (Tables B-1 and B-2) can be represented by

log $(fO_2)_{1,T}(\pm 0.12)^6 = 0.0260 + 0.4381 (10^4/T)$

$$- 0.1572 (10^4/T)^2 (1073 \geq T \geq 873) \quad (10)$$

and are plotted as curve Q in Figure 5.
Ignoring the effect of phase transitions of magnetite and hematite on $\Delta H_{r,8}^0$, linear regression of the data gives

log $(fO_2)_{1,T} (\pm 0.12) = (-28426/T) + 17.036 \quad (11)$

The $\Delta H_{r,8}^0$ derived from equations (7) and (11) is 130.067 kcal, which is about 10 kcal higher than the values plotted in Figure 4.

Taking the effect of phase transitions on $\Delta H_{r,8}^0$ under consideration, the linear regression of the data for $T \geq 950$ yields

log $(fO_2)_{1,T} (\pm 0.12) = (-26629/T) + 15.288, \quad (12)$

which is plotted in Figure 6 as a solid line at $T \geq 950$, with two dotted curves indicating the 95 percent confidence limits of regression. This in turn gives $\Delta H_{r,8}^0 =$

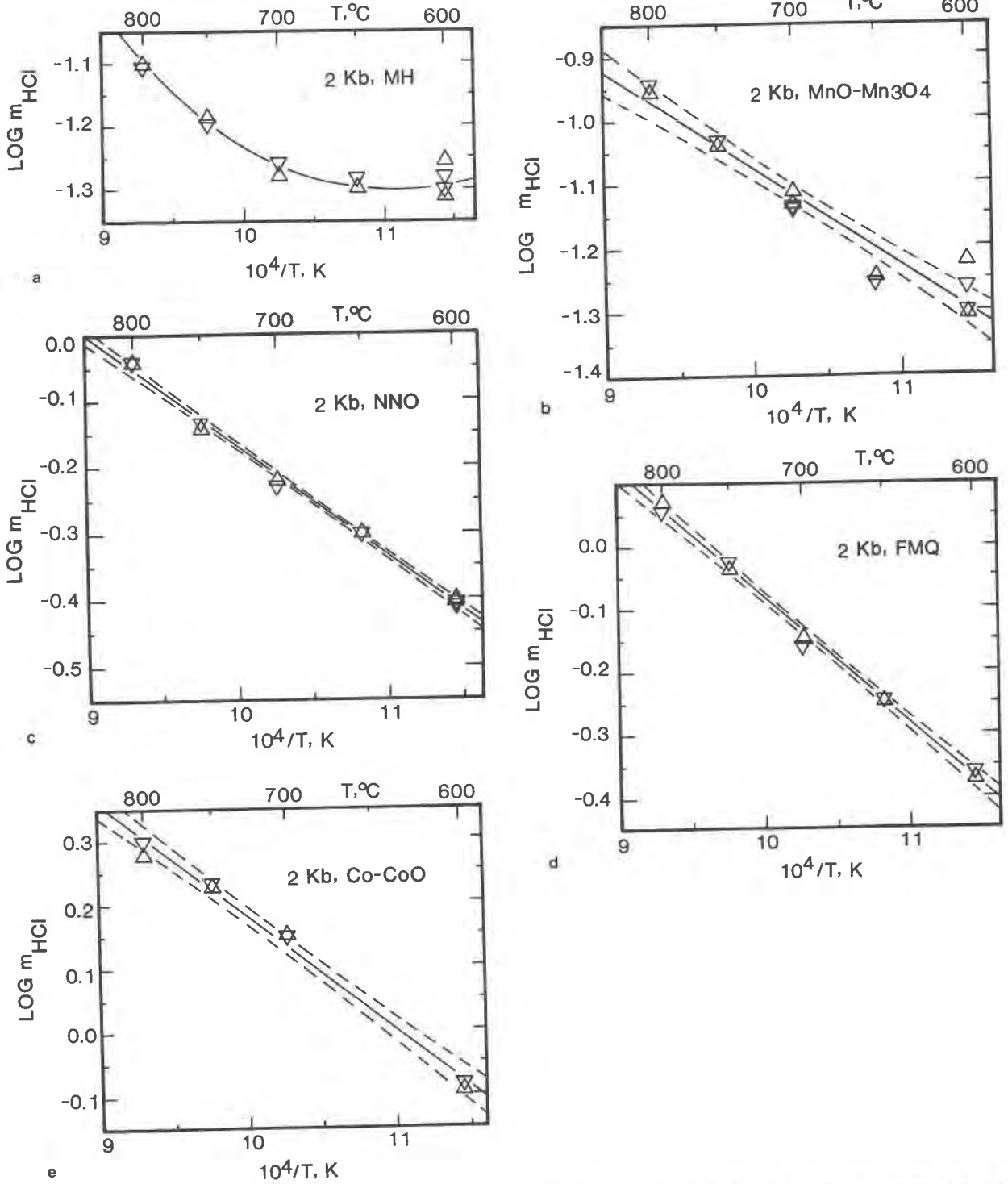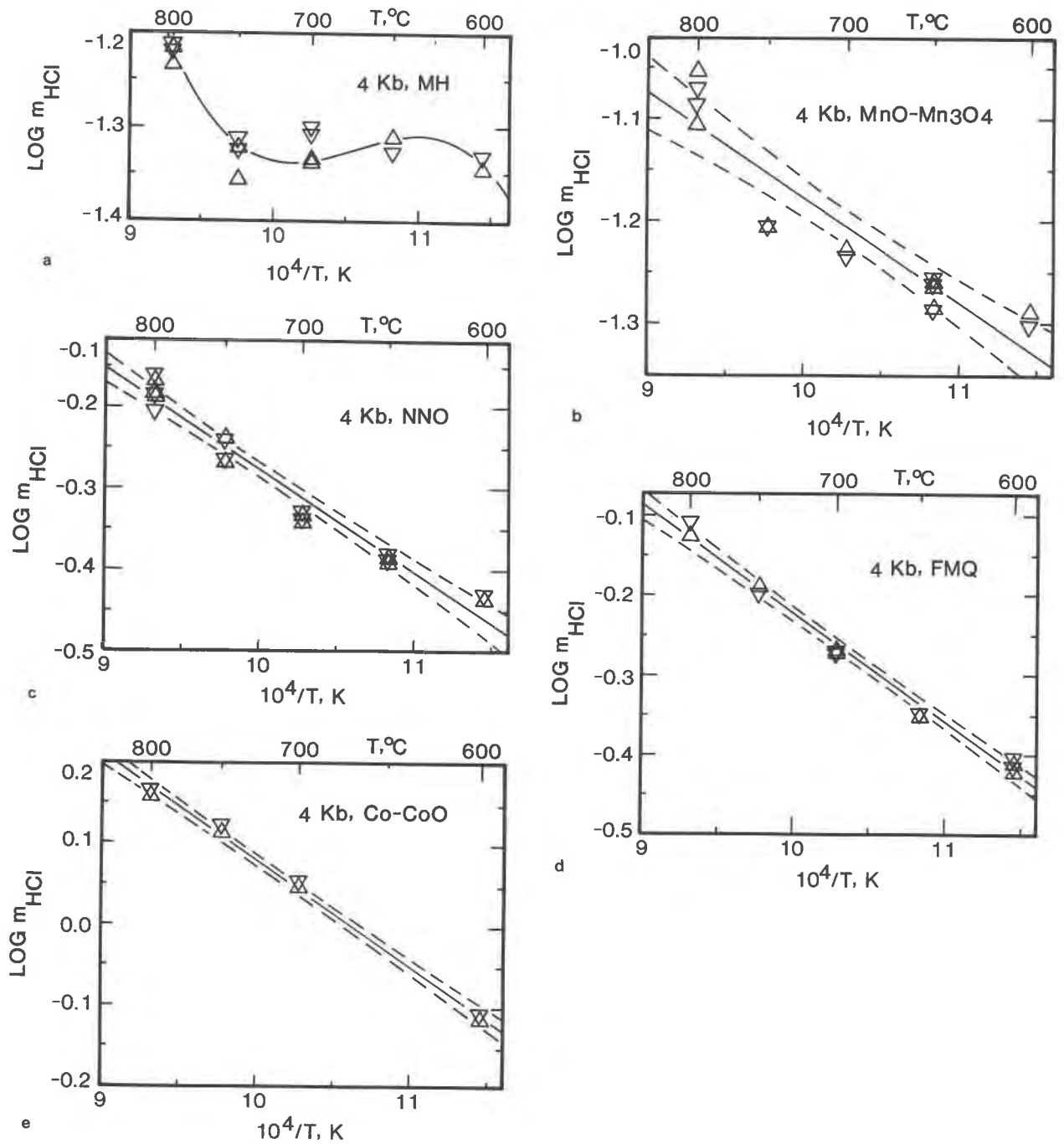[6] For the derivation of uncertainties, see discussion.

Fig. 2. Experimental data for the Ag + AgCl buffer at 2 kbar pressure, using (a) MH + H_2O, (b) MnO + Mn_3O_4 + H_2O, (c) NNO + H_2O, (d) FMQ + H_2O, and (e) Co + CoO + H_2O as external hydrogen buffers. Note that $(mHCl)_{P,T,} = (mCl^-)_{1,25°C}$ [eq. (3)]. Triangles with the apices pointing up and pointing down indicate the average values of log $(mCl^-)_{1,25°C}$ of Table B-1 for sensor A and B respectively. The uncertainties in log $mHCl$ measurement are ±0.02 units for MH and MnO–Mn_3O_4 buffers and ±0.01 units for NNO, FMQ, and Co–CoO buffers. The solid lines are the polynomial (a) and least-squares (b,c,d,e) fit of the data. The dashed curves indicate the 95 percent confidence limits for the regression.

Fig. 3. Experimental data for the Ag + AgCl buffer at ~4 kbar pressure, using (a) MH + H_2O, (b) MnO +Mn_3O_4 + H_2O, (c) NNO + H_2O, (d) FMQ + H_2O, and (e) Co + CoO + H_2O as external hydrogen buffers. Symbols and uncertainties in measurements are as in Fig. 2.

121.844 kcal, which compares with 116 ± 0.72 kcal obtained from the data of Haas and Robie (1973) for $1500 \geq T \geq 1100$. Equation (12) can be extrapolated to higher temperatures. To demonstrate the effect of

the phase transitions on $\Delta H_{r,8}^0$, log fO_2 at 950 K (point A in Fig. 6), obtained from equation (12), together with the data at 650°C gives a linear regression curve of
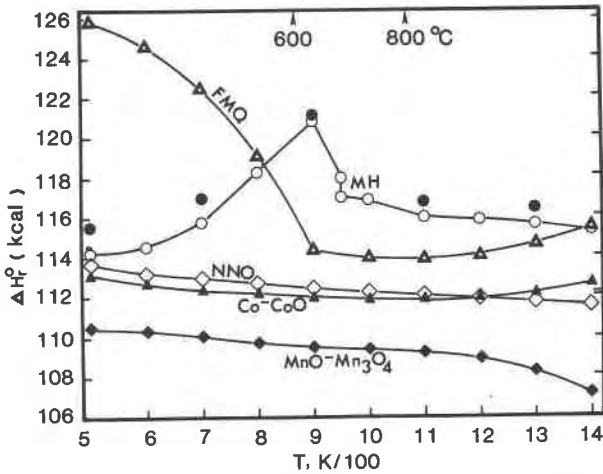
Fig. 4. Standard enthalpy of reaction at 1 atm and T, ΔH_r^0, for the buffer reactions (8), (18), (22), (26), and $2NiO(s) = 2Ni(s) + O_2(g)$, calculated from the data of Robie and Waldbaum (1968), except those indicated by solid circles, which were obtained from the data of Haas and Robie (1973) for MH.

Table 4. Average values for log fO_2 at 1 atm and T^*

| Oxygen Buffer/T, °C	600	650	700	750	800	P (kb)
MH	-15.582	-13.623	-12.012	-10.719	-9.564	2
	-15.540	-13.780	-12.188	-10.580	-9.599	∼4
$MnO-Mn_3O_4$	-15.786	-13.929	-12.717	-11.472	-10.312	2
	-15.918	-14.347	-12.827	-11.396	-10.409	∼4
FMQ	-19.460	-17.965	-16.636	-15.520	-14.388	2
	-19.508	-17.994	-16.598	-15.484	-14.302	∼4
Co-CoO	-20.486	--	-17.776	-16.482	-15.210	2
	-20.498	--	-17.822	-16.564	-15.262	∼4

*Calculated from the values listed in tables B-1 and B-2.

and for $T \geq 1073$,

$$\Delta G_{r,8}^0 (\pm 800) = -69.952\ T + 121,844\ \text{(in cal)} \quad (17)$$

$MnO-Mn_3O_4$ buffer

For the reaction, assuming pure solids

$$2\ Mn_3O_4(s) = 6\ MnO(s) + O_2(g) \quad (18)$$
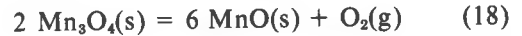
$$K_{18} = fO_2 \quad (19)$$

Experimental results are plotted in Figure 7. Linear regression of the data for $MnO-Mn_3O_4$ (Tables B-1 and B-2) vs. $1/T$ gives

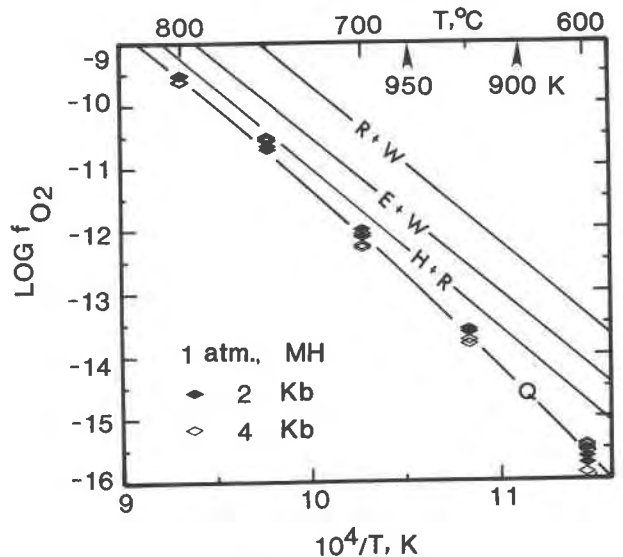$$\log (fO_2)_{1,T} (\pm 0.12) = (-25793/T) + 13.714 \quad (20)$$

$$\log (fO_2)_{1,T} = (-31184/T) + 20.083$$

$$\text{for } 950 \geq T \geq 900 \quad (13)$$

which is plotted as a solid line AB in Figure 6, and yields $\Delta H_{r,8}^0 = 142.686$ kcal. In the same fashion, log fO_2 at 900 K (point B in Fig. 6) is calculated from equation (13), and the linear regression of this value and the 600°C data gives

$$\log (fO_2)_{1,T} = (-29540/T) + 18.257$$

$$\text{for } 900 \leq T \quad (14)$$

which is plotted as a solid line at $T \leq 900$ in Figure 6, and gives $\Delta H_{r,8}^0 = 135.164$ kcal. It should be emphasized that equations (13) and (14), and hence the values for $\Delta H_{r,8}^0$ derived from them, probably have large uncertainties due to the small number of data available. Therefore, equation (10) is preferred in the temperature range investigated, and equation (12) should be used to extrapolate to higher temperatures. For comparison, data of Eugster and Wones (1962), Robie and Waldbaum (1968), and Haas and Robie (1973) are also plotted in Figure 5.

The standard Gibbs free energy of reaction can be obtained by

$$\Delta G_r^0 = -2.303\ RT \log K = -2.303\ RT \log fO_2 \quad (15)$$

Hence, for $1073 \geq T \geq 873$,

$$\Delta G_{r,8}^0 (\pm 590) = -2.303\ RT [0.0260 + 0.4381\ (10^4/T)$$
$$- 0.1572\ (10^4/T)^2]\ \text{(in cal)} \quad (16)$$

Fig. 5. Experimental data of log fO_2 for MH buffer at 1 atm derived from 2 kbar (see Table B-1) and ∼4 kbar (see Table B-2) runs. The solid line Q is the quadratic fit of the data [equation (10)]. Results of previous investigators are also given: E + W is Eugster and Wones (1962): R + W is Robie and Waldbaum (1968); H + R is Haas and Robie (1973).
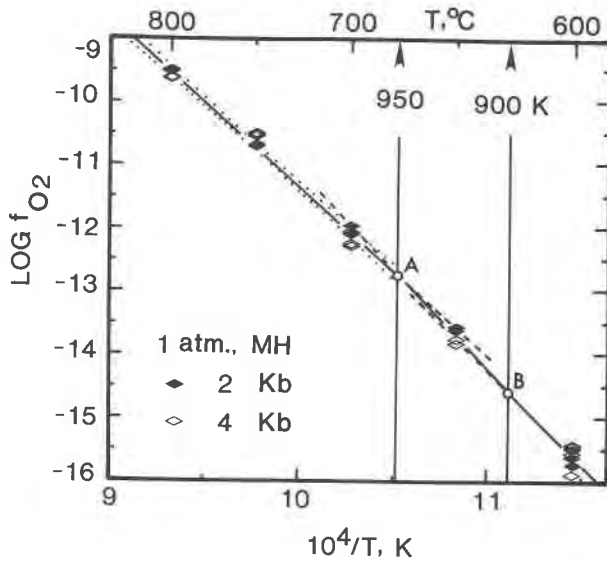
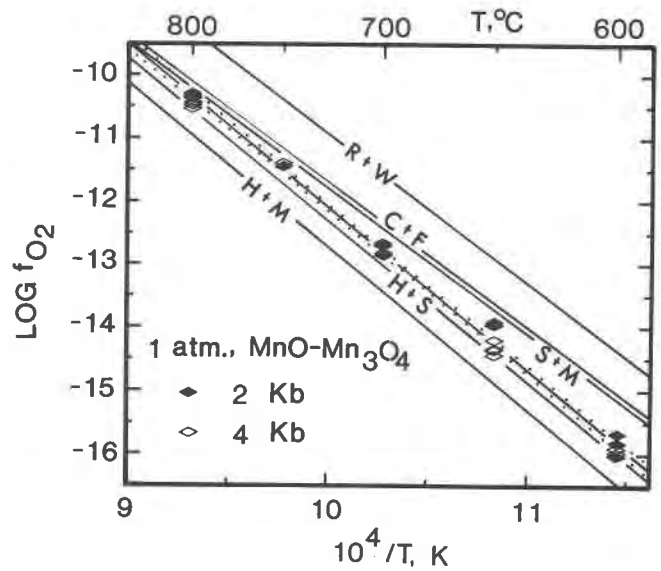Fig. 6. Same data as shown in Fig. 5; for details see text.

Fig. 7. Experimental data of log fO_2 for MnO–Mn_3O_4 buffer at 1 atm derived from 2 kbar (see Table B-1) and ~4 kbar (see Table B-2) runs. The result of the linear regression is shown as a solid line [equation (20)] with two dotted curves indicating the 95 percent confidence limits for the regression. Results of previous investigators are also given: H + M is Hahn and Muan (1960); S + M is Schwerdtfeger and Muan (1967); C + F is Charette and Flengas (1968); R +W is Robie and Waldbaum (1968); H + S is Huebner and Sato (1970). The result of Blumenthal and Whitmore (1961) almost coincides with the line S + M.

which is shown in Figure 7 as a solid line with two dotted curves indicating the 95 percent confidence limits for the regression. Also plotted are the results of Hahn and Muan (1960), Blumenthal and Whitmore (1961), Schwerdtfeger and Muan (1967), Charette and Flengas (1968), Robie and Waldbaum (1968), and Huebner and Sato (1970). Equation (20) gives $\Delta H^0_{r,18}$ = 118.019 kcal, which compares to 117.7±1.6 kcal of Huebner and Sato (1970). The agreement is excellent. The free energy of reaction can be represented by the equation (in cal)

$$\Delta G^0_{r,18} \ (\pm 590) = -62.749 \ T + 118{,}019 \quad (21)$$

For the data of previous investigators, the reader is referred to Huebner and Sato (1970).

FMQ buffer

For the reaction, assuming pure solids

$$2 \ Fe_3O_4(s) + 3 \ SiO_2(s) = 3 \ Fe_2SiO_4(s) + O_2(g) \quad (22)$$
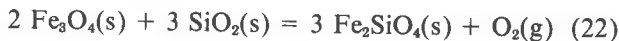
$$K_{22} = fO_2 \quad (23)$$

Experimental results were plotted in Figure 8, together with the data of Eugster and Wones (1962), Wones and Gilbert (1969), and Hewitt (1976). Linear regression of the fO_2 data for FMQ (Tables B-1 and B-2) *vs.* $1/T$ gives

$$\log(fO_2)_{1,T} \ (\pm 0.08) = (-23973/T) + 7.985 \quad (24)$$

which is about 0.6–1.1 and 0.3–0.5 log units higher than those given by Wones and Gilbert (1969) and Hewitt (1976) respectively (Fig. 8). The $\Delta H^0_{r,22}$ is
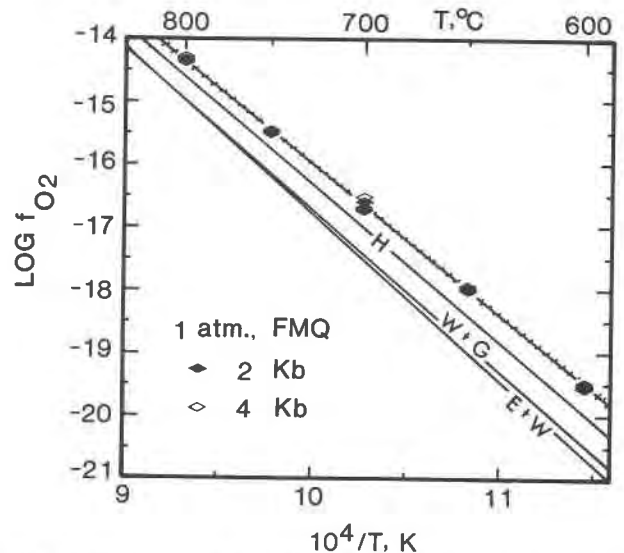

Fig. 8. Experimental data of log fO_2 for FMQ buffer at 1 atm derived from 2 kbar (see Table B-1) and ~4 kbar (see Table B-2) runs. Linear regression of the data gives the solid line [equation (24)] with two dotted curves indicating the 95 percent confidence limits. Results of Eugster and Wones (1962) (E + W), Wones and Gilbert (1969) (W + G), and Hewitt (1976) (H) are also plotted.

109.692 kcal, which compares with 117.8 ± 2.5 kcal of Wones and Gilbert (1969) and 114.7 ± 2.8 kcal of Hewitt (1976). The free energy of reaction is given by the equation (in cal)

$$\Delta G^0_{r,22} (\pm400) = -36.536\ T + 109,629 \quad (25)$$

The fO_2 values for FMQ buffer given by Wones and Gilbert (1969) and Hewitt (1976) were obtained by using the "Shaw bomb" (Shaw, 1963, 1967). There are many inherent problems in this particular apparatus (Hewitt, 1977). The H_2 leakage from the bomb is the most serious one, because it prevents equilibration of fH_2 between the bomb and membrane, even though a steady state can be maintained. Since the measured H_2 pressure inside the membrane is always higher than that of the bomb and sample for the steady state, the reported fO_2 values tend to be lower than the equilibrium ones.

The FMQ buffer reaction has recently been reversed at 1 atm and 1395 K by Williams (personal communication) using a gas-mixing furnace, in which fO_2 was controlled by mixing CO and CO_2, monitored by a $(ZrO_2)_{0.85}(CaO)_{0.15}$ ceramic oxygen electrolyte cell (Sato, 1971; Williams and Mullins, 1976). His log fO_2 value for FMQ buffer is -9.30 ± 0.02, which compares with -9.20 calculated from equation (24).

The fO_2 values of this study for FMQ buffer are consistently higher than those calculated from ther-mochemical data, whereas those for MH buffer are consistently lower (see Figs. 5 and 8). This discrepancy can be minimized by adopting new Gibbs free energy of formation values for magnetite ($\Delta G^0_{f,Fe3O4}$), since magnetite appears on the different sides of the reaction in reactions (8) and (22). Assuming the Gibbs free energy of formation data for hematite, fayalite, and quartz given by Robie and Waldbaum (1968) to be correct, values for $\Delta G^0_{f,Fe3O4}$ are calculated from equations (16), (17), and (25), and listed in Table 5. Values obtained from FMQ buffer are 1.0–1.4 kcal/mole less negative than those derived from MH buffer. This discrepancy is due to the uncertainties in the free-energy data for hematite, fayalite, and quartz. Since there is one less solid phase involved in MH buffer reaction than in that of FMQ, and the free-energy data for hematite reported by Haas and Robie (1973) are in good agreement with those of Robie and Waldbaum (1968), values for $\Delta G^0_{f,Fe3O4}$ derived from MH buffer (in Table 5) are preferred. They are about 2 kcal/mole less negative than those of Robie and Waldbaum (1968). Using the free-energy data of Haas and Robie (1973) for hematite, the calculated free-energy values for magnetite are 0.68, 0.35, and 0.17 kcal/mole less negative than theirs at 900, 1100, and 1300 K respectively.

Values for $\Delta G^0_{f,Fe3O4}$ derived from equation (25) and the equilibrium constant for iron–quartz–fayalite (IQF) buffer assemblage, K_{fa}, given by Williams

Table 5. Calculations of standard Gibbs free energy of formation for magnetite at 1 atm and T

T, K	$\Delta G^0_{r,8}$ [1]	$\Delta G^0_{f,Fe_3O_4}$ [2]	$\Delta G^0_{f,Fe_3O_4}$ [3]	$\Delta G^0_{r,22}$ [4]	$\Delta G^0_{f,Fe_3O_4}$ [5]	$\Delta G^0_{f,Fe_3O_4}$ [6]	$\Delta G^0_{f,Fe_3O_4}$ [7]	$\Delta G^0_{f,Fe_3O_4}$ [8]
900	59.769*	-195.461	-195.553	76.810	-194.426	-186.231	-197.473	-196.23
1000	51.764*	-188.633	---	73.156	-187.369	-180.601	-190.506	---
1100	44.897	-181.496	-181.646	69.502	-180.205	-174.972	-183.445	-182.00
1200	37.902	-174.368	---	65.849	-173.041	-169.343	-176.370	---
1300	30.906	-167.263	-167.398	62.195	-165.879	-163.714	-169.294	-167.57

1) ±0.590 kcal; calculated from eq. (16) (indicated by stars) and eq. (17).

2) ±0.613 kcal/mole; calculated from $\Delta G^0_{r,8}$ and $\Delta G^0_{f,Fe_2O_3}$ data of Robie and Waldbaum (1968).

3) Same as 2) except $\Delta G^0_{f,Fe_2O_3}$ data of Haas and Robie (1971) were used.

4) ±0.400 kcal; calculated from eq. (25).

5) ±1.895 kcal/mole; calculated from $\Delta G^0_{r,22}$, and the data of $\Delta G^0_{f,Fe_2SiO_4}$ and $\Delta G^0_{f,SiO_2}$ from Robie and Waldbaum (1968).

6) ±0.245 kcal/mole; calculated from eq. (C-5) (Appendix C).

7) ±0.510 kcal/mole; from Robie and Waldbaum (1968).

8) In kcal/mole; from Haas and Robie (1973).

(1971) are also tabulated in Table 5 (for calculations, see Appendix C). They are 9.2 and 3.5 kcal/mole less negative than the preferred values at 900 and 1300 K respectively. These large discrepancies are due to the small K_{ra} values obtained when his data are extrapolated to lower temperatures. These discrepancies are probably too large and thus suggest that the ΔH_r^0 from Williams (1971) is too small.

Co-CoO buffer

For the reaction, assuming pure solids

$$2 \text{ CoO(s)} = 2 \text{ Co(s)} + \text{O}_2\text{(g)} \qquad (26)$$
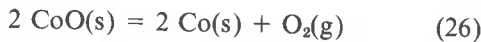
$$\log K_{26} = \log f\text{O}_2 \qquad (27)$$

Experimental results are plotted in Figure 9. Linear regression of the $f\text{O}_2$ data (Tables B-1 and B-2) vs. $1/T$ yields

$$\log (f\text{O}_2)_{1,T} \ (\pm 0.08) = (-24391/T) + 7.382\,(28)$$

which is about 0.2 log units less negative than those of Robie and Waldbaum (1968). The $\Delta H_{r,26}^0$ is 111.604 kcal, which compares with 111.940 and 111.808 kcal of Robie and Waldbaum (1968) for 900 and 1100 K respectively. The standard free energy of formation for CoO can be derived from the equation

$$
\begin{aligned}
\Delta G_{f,CoO}^0(\pm 200) &= -0.5\ \Delta G_{r,26}^0 \\
&= 16.889\ T - 55{,}802\ \text{(cal)} \qquad (29)
\end{aligned}
$$

The values calculated from equation (29) are 0.36 and 0.46 kcal less negative than those of Robie and Waldbaum (1968) at 900 and 1300 K respectively.

Equations for log $(f\text{O}_2)_{P,T}$ of the buffers investigated are summarized in Table 6. The equations given by the previous investigators are also tabulated.

$f\text{H}_2$ measurements of the pressure vessels

The $f\text{H}_2$ sensor technique provides a method to measure the $f\text{H}_2$ of a hydrothermal system. For example, the $f\text{H}_2$ of the internally-heated pressure vessels A and B used in this study [see footnote (1) of Table B-2] were measured at ~4 kbar and 600°, 700°, and 800°C. The results, given in Table B-2 (run no. INT-1 to INT-7), indicate that both pressure vessels A and B have $f\text{H}_2$ values between that of MnO–Mn_3O_4–H_2O and NNO–H_2O buffers. The $f\text{H}_2$ values of the pressure vessels depend on the $f\text{O}_2$ of the vessels and the H_2O content of the pressure medium (Ar). Since the same Ar gas was used in vessels A and B, the higher $f\text{H}_2$ in vessel B indicates that it has a lower $f\text{O}_2$ [see equation (A-2)]. Since the mass of the pressure vessels is large compared to that of the sample charges, each pressure vessel probably has a large buffer capacity for $f\text{O}_2$, which depends on the types of material used for the vessel, its furnace wind-
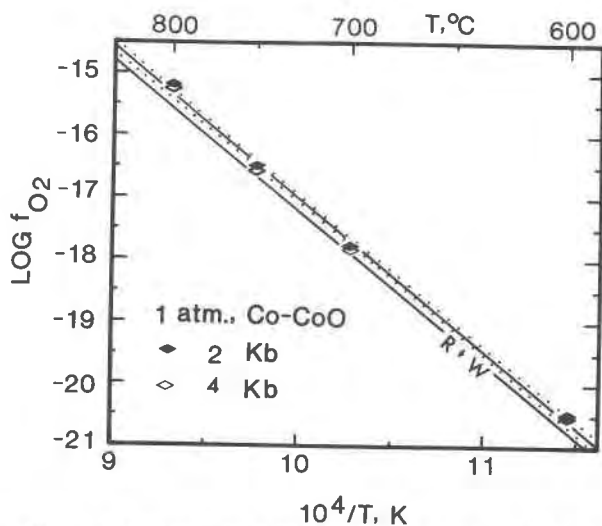

Fig. 9. Experimental data of log $f\text{O}_2$ for Co–CoO buffer at 1 atm derived from 2 kbar (see Table B-1) and ~4 kbar (see Table B-2) runs. Linear regression of the data gives the solid line [equation (28)] with two dotted curves indicating the 95 percent confidence limits. Free-energy data of Robie and Waldbaum (1968) yield the line R + W.

Table 6. Calculations of log $f\text{O}_2$ at P and T. log $(f\text{O}_2)_{P,T} = A/T + B + C(P-1)/T$

Buffer	A	B	C*	Sources of Data
MH	−26629	15.288	0.019	(1),(9)
	(713)	(0.698)		
	−25632	14.602		(2)
	−24912	14.41		(3)
	−25344	15.669		(8)
MnO-Mn₃O₄	−25793	13.714	0.081	(1)
	(317)	(0.330)		
	−25680	13.38		(4)
	−23234	11.56		(5)
NNO	−24930	9.36	0.046	(4)
	−24405	8.867		(5)
	−24709	8.94		(3)
FMQ	−23973	7.985	0.092	(1)
	(165)	(0.172)		
	−25056	8.74		(6)
	−25738	9.00		(7)
	−26494	9.69		(3)
Co-CoO	−24391	7.382	0.052	(1)
	(325)	(0.333)		
	−24433	7.254		(8)

*C = −ΔV_s/2.303 R; molar volume data for solids are from Robie and Waldbaum (1968).

(1) Calculated from the values listed in tables B-1 and B-2; standard errors are given in parentheses. (2) Calculated from Haas and Robie (1973). (3) Eugster and Wones (1962). (4) Huebner and Sato (1970). (5) Calculated from Charette and Flengas (1968). (6) Hewitt (1976). (7) Wones and Gilbert (1969). (8) Calculated from Robie and Waldbaum (1968). (9) For T ≥ 950 K; for explanation, see text.

ings, and also on its history of usage. If this type of pressure vessel is used to investigate mineral–solution or mineral–liquid equilibria involving redox reactions, it is important to know the fO_2 and fH_2 of the vessel for experiments performed in an open capsule and a closed Pt capsule respectively.

Discussion

The internal consistency of the thermodynamic data for oxygen buffers can be checked by using the fH_2 sensor technique. The fO_2 values obtained in this report are based on the assumption that those reported by Huebner and Sato (1970) for the NNO buffer are correct. Therefore, the actual value for fO_2 might change if one would choose a different set of data as reference. However, the relative position of the buffer curve in $\log fO_2 - 1/T$ space will remain unchanged. The advantages of using a reference are that any systematic errors involved in (1) the measurements of intensive parameters, such as P, T, and $(mCl^-)_{1,25°C}$, (2) the assumption for ideal mixing of HCl and H_2O at P and T [see equation (A-5)], and (3) the simplifications in calculation such as in equations (A-1) and (A-6), tend to cancel out, and the thermochemical uncertainties in $(K_4)_{P,T}$, $(K_W)_T$, and fH_2O can be eliminated. These can be shown in the following relation (for the derivation, see Appendix D):

$$\log (fO_2^S)_{P,T} \approx \log (fO_2^R)_{P,T} + 4 \log (mCl^-)_{1,25°C}^R$$
$$- 4 \log (mCl^-)_{1,25°C}^S \quad (30)$$

where the superscripts R and S indicate reference and sample run respectively.

The uncertainties in $\log (mCl^-)_{1,25°C}$ measurements are about ± 0.02 for MH and MnO–Mn$_3$O$_4$ buffers, and ± 0.01 for NNO, FMQ and Co–CoO buffers. Therefore, from equation (30), the uncertainties in $\log fO_2$ given in Tables B-1 and B-2 are ± 0.12 for MH and MnO–Mn$_3$O$_4$ buffers, and ± 0.08 for FMQ and Co–CoO buffers, without considering that associated with the reference (NNO) buffer.

To test the internal consistency of the data, the following relation was derived from equation (4):

$$\log (mCl^-)_{1,25°C} = (1/2) \log (fH_2)_{P,T}$$
$$- \log (K_4)_{P,T} \quad (31)$$

The calculated values of $\log fH_2$ for each buffer at 2 kbar and 700°C are listed in Table 7. The measured values for $\log (mCl^-)_{1,25°C}$ [from Table B-1(c)] are plotted against the calculated $\log fH_2$ in Figure 10. If the data are internally consistent, from equation (31), all data points should lie on a straight line with a

Table 7. Calculated values for log fH_2 at 2 kbar, 700°C

Buffer	log f_{O_2} [1]	Sources of [2] Data	log f_{H_2} [3]
MH	-11.685	(2)	-1.480
	-11.154	(3)	-1.745
	-10.339	(8)	-2.152
MnO-Mn$_3$O$_4$	-12.846	(4)	-0.899
	-12.152	(5)	-1.246
NNO	-16.167	(4)	0.762
FMQ	-16.822	(6)	1.089
	-17.263	(7)	1.310
	-17.350	(3)	1.353
Co-CoO	-17.750	(8)	1.553

1) Calculated from equations given in table 6.

2) See footnotes of table 6.

3) Calculated from eq. (A-2); for sources of data; see footnotes (2) and (3) of table 2.

slope of 0.5 and an intercept of $-\log (K_4)_{P,T}$. It is clear from Figure 10 that to make the data internally consistent the MH and FMQ buffers should be more reducing and oxidizing, respectively, than previously reported. The most recent data for MH and FMQ buffers tend to fulfill the internal consistency. The good agreement between the values of this study and those of Huebner and Sato (1970) for MnO–Mn$_3$O$_4$ and Robie and Waldbaum (1968) for Co–CoO buffers indicates that the present calibration method is applicable in this fO_2 range. For more reducing conditions, Ag–AgBr and Ag–AgI buffers of Chou and Eugster (1976b) should give better results.
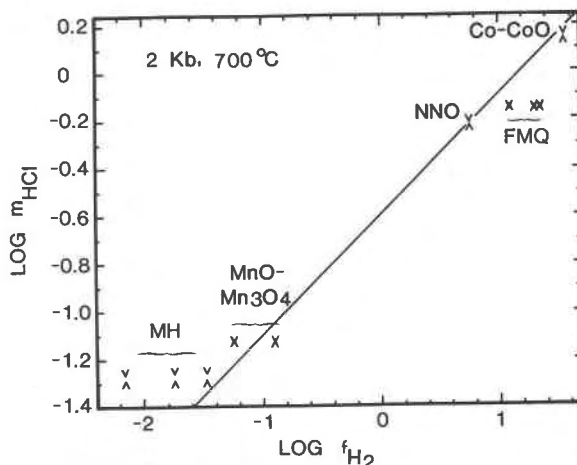

Fig. 10. Test of the internal consistency of the previous thermodynamic data at 2 kbar and 700°C. Values for log mHCl are those of log $(mCl^-)_{1,25°C}$ in Table B-1. The calculated values of log fH_2 are from Table 7. For details see text. Symbols $\wedge$ and $\vee$ represent data from sensor A and B respectively.

Conclusion

With a slight modification, the Ag–AgCl–H_2O–HCl acid buffer developed by Frantz and Eugster (1973) has been used as a sensor for fH_2 in hydrothermal experiments. The concentration of HCl in the sensor, which can be measured after quench, is related to the $(fH_2)_{P,T}$ of the system by equation (4). The oxygen-buffer technique of Eugster (1957) and the hydrogen-osmosis technique of Shaw (1963, 1967) are two different ways of imposing a constant fH_2 onto a hydrothermal system and controlling its oxidation state, whereas the fH_2 sensor technique can be used to determine the oxidation state of a hydrothermal system by measuring its fH_2. The advantage of using the fH_2 sensor is that the equilibrium of the entire system is achieved much more rapidly, because the mass of hydrogen transferred between the charge and sensor is minimized.

The fH_2 sensor technique has many applications (Chou and Eugster, 1976a; Wood et al., 1975; Chou and Williams, 1977). The internal consistency of the thermodynamic data for the standard oxygen buffers, including MH, MnO–Mn_3O_4, NNO, FMQ, and Co–CoO, has been tested in this paper at 2 and 4 kbar total pressures and between 600° and 800°C. A set of internally consistent data for these buffers has been suggested, with the data for NNO buffer given by Huebner and Sato (1970) as a reference. The present fO_2 values for MnO–Mn_3O_4 and Co–CoO buffers are in good agreement with those of Huebner and Sato (1970) and Robie and Waldbaum (1968) respectively. However, for MH and FMQ buffers, the present fO_2 values are consistently lower and higher respectively than those reported previously. These discrepancies yield new values for $\Delta G^{\circ}_{f,Fe_3O_4}$, which are somewhat less negative than those of Haas and Robie (1973).

Acknowledgments

References

Blumenthal, R. N. and D. H. Whitmore (1961) Electrochemical measurements of elevated temperature thermodynamic properties of certain iron and manganese oxide mixtures. J. Am. Ceram. Soc., 44, 508–512.

Burnham, C. W., J. R. Holloway and N. F. Davis (1969) Thermodynamic properties of water to 1000°C and 10,000 bars. Geol. Soc. Am. Spec. Pap. 132.

Charette, G. G. and S. N. Flengas (1968) Thermodynamic properties of the oxides of Fe, Ni, Pb, Cu, and Mn by EMF measurements. J. Electrochem. Soc., 115, 796–804.

Chou, I.-M. and H. P. Eugster (1976a) A sensor for hydrogen fugacities at elevated P and T and applications (abstr.). Trans. Am. Geophys. Union, 57, 340.

—— and —— (1976b) Fugacity control and dissociation constants of HBr and HI. Contrib. Mineral. Petrol., 56, 77–100.

—— and —— (1977) Solubility of magnetite in supercritical chloride solutions. Am. J. Sci., 277, 1296–1314.

—— and J. D. Frantz (1977) Recalibration of Ag + AgCl buffer at elevated pressures and temperatures. Am. J. Sci., 277, 1067–1072.

—— and R. J. Williams (1977) Activity of H_2O in CO_2–H_2O at 600°C and pressure to 8 kilobars (abstr.) Geol. Soc. Am. Abstracts with Programs, 9, 928.

——, H. P. Eugster, P. Berens and J. H. Weare (1978) Diffusion of hydrogen through platinum membranes at high pressures and temperatures. Geochim. Cosmochim. Acta, 42, 281–288.

Eugster, H. P. (1957) Heterogeneous reactions involving oxidation and reduction at high pressures and temperatures. J. Chem. Phys., 26, 1760–1761.

—— and D. R. Wones (1962) Stability relations of the ferruginous biotite, annite. J. Petrol., 3, 81–124.

—— and G. B. Skippen (1967) Igneous and metamorphic reactions involving gas equilibria. In P. H. Abelson, Ed., Researches in Geochemistry, Vol. 2, p. 377–396. Wiley, New York.

Frank, E. U. (1956) Hochverdichteter Wasserdampf III. Ionendissoziation von HCl, KOH und H_2O in überkritisches Wasser als elektrolytisches Lösungsmittel. Angew. Chem., 73, 309–322.

Frantz, J. D. (1973) Acid Buffers: use of Ag + AgCl for measuring mineral–solution equilibria in the system MgO–SiO_2–H_2O–HCl. Ph.D. Thesis, Johns Hopkins University, Baltimore.

—— and H. P. Eugster (1973) Acid-base buffers: use of Ag + AgCl in the experimental control of solution equilibria at elevated pressures and temperatures. Am. J. Sci., 273, 268–286.

Gunter, W. D. (1974) An experimental study of mineral–solution equilibria applicable to metamorphic rocks. Ph.D. Thesis, Johns Hopkins University, Baltimore.

—— and H. P. Eugster (in press) Wollastonite solubility and free energy of supercritical aqueous $CaCl_2$. Contrib. Mineral. Petrol.

Haas, J. L. and R. A. Robie (1973) Thermodynamic data for wüstite, $Fe_{0.947}O$, magnetite, Fe_3O_4 and hematite, Fe_2O_3 (abstr.). *Trans. Am. Geophys. Union, 54*, 483.

Hahn, W. C., Jr. and A. Muan (1960) Studies in the system Mn–O: the Mn_2O_3–Mn_3O_4 and Mn_3O_4–MnO equilibria. *Am. J. Sci., 258*, 66–78.

Helgeson, H. C. and D. H. Kirkham (1976) Theoretical prediction of the thermodynamic properties of aqueous electrolytes at high pressures and temperatures, III. Equation of state for aqueous species at infinite dilution. *Am. J. Sci., 267*, 97–240.

Hewitt, D. A. (1976) A redetermination of the fayalite–magnetite–quartz equilibrium between 650 and 850°C (abstr.). *Trans. Am. Geophys. Union, 57*, 1020.

—— (1977) Hydrogen fugacities in Shaw bomb experiment. *Contrib. Mineral. Petrol., 65*, 165–169.

Huebner, J. S. (1971) Buffering techniques for hydrostatic systems at elevated pressures. In G. C. Ulmer, Ed., *Research Techniques for High Pressure and High Temperature*, p. 123–177. Springer-Verlag, New York.

—— and M. Sato (1970) The oxygen fugacity–temperature relationships of manganese oxide and nickel oxide buffers. *Am. Mineral., 55*, 934–952.

Lewis, G. N. and M. Randall (1923) *Thermodynamics*. McGraw-Hill, New York.

Robie, R. A. and D. R. Waldbaum (1968) Thermodynamic properties of minerals and related substances of 298.15°K (25.0°C) and one atmosphere (1.013 bars) pressure and at higher temperatures. *U. S. Geol. Surv. Bull. 1259*.

Rudert, V., I.-M. Chou and H. P. Eugster (1976) Temperature gradients in rapid-quench cold-seal pressure vessels. *Am. Mineral., 61*, 1012–1015.

Sato, M. (1971) Electrochemical measurements and control of oxygen fugacity and other gaseous fugacities with solid electrolyte sensors. In G. C. Ulmer, Ed., *Research Techniques for High Pressure and High Temperature*, p. 43–99. Springer-Verlag, New York.

Schwerdtfeger, K. and A. Muan (1967) Equilibria in the system Fe–Mn–O involving "(Fe,Mn)O" and $(Fe,Mn)_3O_4$ solid solutions. *Trans. AIME, 239*, 1114–1119.

Shaw, H. R. (1963) Hydrogen–water vapor mixtures: control of hydrothermal atmospheres by hydrogen osmosis. *Science, 139*, 1220–1222.

—— (1967) Hydrogen osmosis in hydrothermal experiments. In P. H. Abelson, Ed., *Researches in Geochemistry, Vol. 2*, p. 521–541. Wiley, New York.

Williams, R. J. (1971) Reaction constants in the system Fe–MgO–SiO_2–O_2 at 1 atm between 900° and 1300°C: experimental results. *Am J. Sci., 270*, 334–360.

—— and O. Mullins (1976) A system using solid ceramic oxygen electrolyte cells to measure oxygen fugacities in gas-mixing system. *NASA Tech. Memorandum, NASA TM X-58167*.

Wones, D. R. and H. P. Eugster (1965) Stability of biotite: experiment, theory, and application. *Am. Mineral., 50*, 1228–1272.

—— and M. C. Gilbert (1969) The fayalite–magnetite–quartz assemblage between 600° and 800°C. *Am. J. Sci., 267-A*, 480–488.

—— (1972) Stability of biotite: A reply. *Am. Mineral., 57*, 316–317.

Wood, J. R., I.-M. Chou and W. D. Gunter (1975) Thermodynamics of supercritical brines: some new experimental techniques (abstr.). *Geol. Soc. Am. Abstracts with Programs, 7*, 1321.

Zen, E-an (1977) The phase-equilibrium calorimeter, the petrogenetic grid, and a tyranny of numbers. *Am. Mineral., 62*, 189–204.